

Influence of electrical fatigue on hole transport in poly(*p*-phenylenevinylene)-based organic light-emitting diodes

Katja Stegmaier,^{a)} Arne Fleissner, Helga Janning, Sergey Yampolskii, Christian Melzer, and Heinz von Seggern

Electronic Materials Department, Institute of Materials Science, TU Darmstadt, Petersenstraße 23, 64287 Darmstadt, Germany

(Received 28 February 2011; accepted 14 June 2011; published online 8 August 2011)

The hole transport in poly(*p*-phenylenevinylene) (PPV) was investigated before and after bipolar electrical stress by the time-of-flight (TOF) method. Bipolar structures similar to organic light emitting diodes (OLEDs) were realized, yet with much thicker layers than usually prevailing in OLEDs. During fatigue, the hole mobility is reduced, the field dependence of the mobility is increased, and the hole transport becomes more and more dispersive. These results go along with the fatigue behavior of thin film OLEDs that were investigated by charge extraction via linearly increasing voltage (CELIV). Even though theoretical simulations could show that both thick- and thin-film PPV-based OLED structures are dominated by holes, the presented results indicate that the existence of electrons leads to degradation during hole transport. A possible reason for an enlarged electron density in the otherwise hole dominated device is suggested. © 2011 American Institute of Physics. [doi:10.1063/1.3610381]

I. INTRODUCTION

Advantages of polymer light-emitting diodes (PLEDs) compared to small molecule organic light emitting diodes (SM-OLEDs) are their easy and cheap processability from solution and their suitability for large-area applications.¹ Problems regarding stability and lifetime of PLEDs have still to be overcome and are reasons why SM-OLEDs have displaced PLEDs in commercial applications almost completely.¹ Therefore, it is necessary to investigate fatigue of PLEDs.

One of the most prominent and well-known representatives of polymer semiconductors are poly(*p*-phenylenevinylene) (PPV) derivatives.²⁻⁴ However, organic light-emitting diodes (OLEDs) comprising such polymeric semiconductors still disclose a degradation of the device performance under device operation, limiting their applicability. During operation, the luminescence fades whereas the impedance increases.⁵ Up to now, the processes responsible for this device fatigue are not fully understood. Electrochemical degradation of electrodes,⁶ crystallization of the PPV layer,⁷ and photo-oxidation of the polymer backbone⁸⁻¹¹ with indium tin oxide (ITO) as a possible source of oxygen have been identified as relevant mechanisms occurring during device stressing but can now partly be eliminated. Since a change of the electrode or the injection properties during fatigue has then been ruled out^{5,12} the focus retained on the change in the carrier transport properties of the PPV-based devices. Parker *et al.*⁵ postulated a decrease in electron mobility but no change in hole mobility by taking into account the increase rate of the external voltage during electrical stressing of unipolar PPV-based diodes. Dane and Gao¹³ claimed a change in electron mobility, too. They monitored the position of the

recombination zone in planar PPV-based electrochemical cells and concluded from a shift of the recombination zone towards the cathode after electrical stress a degraded electron mobility. Until today a direct proof of the persistency of the hole mobility against fatigue is still missing and only unipolar but no bipolar stress was applied.

Here we investigate the evolution of the hole mobility during fatigue of bipolar diodes by means of the time-of-flight (TOF) method. Our results show in the contrary to the earlier publications that the hole mobility decreases during device operation. It is discussed to what extent the thus investigated fatigue of the bipolar TOF samples can be compared to real OLEDs, and a possible reason behind the observed degradation of the hole mobility is suggested.

II. EXPERIMENTAL

Three different PPV derivatives used as semiconductor layers in single layer OLEDs are used in this work. The PPV derivatives differ in their side chains: the well-known poly[2-methoxy-5-(3',7'-dimethyloctyloxy)-1,4-phenylenevinylene] (OC₁C₁₀-PPV) with its strongly asymmetric side chains, poly[2-propoxy-5-(2'-ethylhexyloxy)-1,4-phenylenevinylene] (OC₃C₈-PPV) with less asymmetry in the side chains, and the symmetric poly[2,5-bis(2-ethylhexyloxy)-phenylenevinylene] (OC₈C₈-PPV). The respective chemical structures are depicted in the insets of Fig. 1.

All samples were fabricated in nitrogen atmosphere. Four different device structures were produced: indium tin oxide (ITO)/poly(styrenesulfonate)-doped poly(3,4-ethylenedioxythiophene) (PEDOT:PSS)/PPV/Ca/Al (the inset of Fig. 4 shows the energetic scheme), ITO/PEDOT:PSS/OC₈C₈-PPV/Au (the inset of Fig. 7 shows the energetic scheme), ITO/PEDOT:PSS/OC₈C₈-PPV/Al, and Al/OC₈C₈-PPV/Al. The PPV-derivatives were spin coated from toluene solution

^{a)}Electronic mail: stegmaier@e-mat.tu-darmstadt.de.

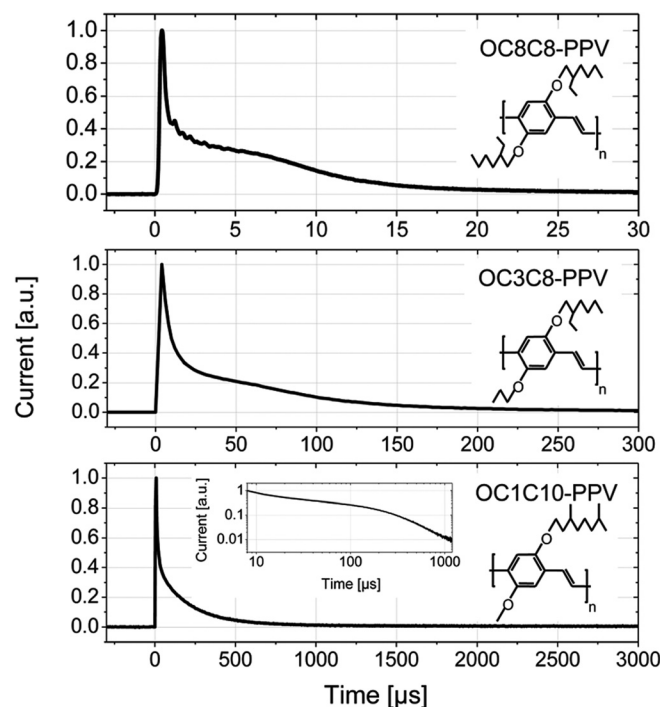


FIG. 1. Hole current transients for three different PPV derivatives OC₈C₈, OC₃C₈, and OC₁C₁₀-PPV. The time-of-flight measurements were carried out on diodes with calcium and ITO/PEDOT:PSS as electrodes at a reverse bias of 40 V. The PPV layer thicknesses were 1.7 μm for OC₈C₈-PPV and 2.0 μm for OC₁C₁₀ and OC₃C₈-PPV. The insets show the chemical structure of the investigated polymers and the double logarithmic plot of the hole current transient of OC₁C₁₀-PPV based diodes.

with a concentration of 8 mg/ml or 25 mg/ml at 3000 rpm for 30 s or 600 s, resulting in film thicknesses of 130 nm or around 2000 nm, respectively. The semitransparent cathode stacks were deposited by thermal evaporation at a deposition rate of 2 $\text{\AA}/\text{s}$ and a base pressure of 10^{-6} mbar.

All experiments were performed at room temperature in inert nitrogen atmosphere. Fatiguing of OLEDs was performed by applying constant current densities ($j = 10, 50, \text{ or } 100 \text{ mA}/\text{cm}^2$). During fatiguing a Keithley-2000 multimeter monitored the driving voltage of the OLED and the electroluminescence was measured with a silicon photodiode. To provoke additional photoluminescence, the OLEDs were excited every 60 s for 5 s with UV light. Alternatively, the TOF samples were stressed by applying a constant voltage with a HP4145A parameter analyzer and then the driving current was monitored. Optical stressing of samples was performed using commercial inorganic light emitting diodes with wavelengths of 516 nm and 572 nm, respectively. The emission wavelength of the first diode is located in the fundamental absorption of all three PPV derivatives; the wavelength of the latter diode is spectrally located in the overlap between emission and absorption spectra. The LEDs irradiated through the semitransparent cathode stacks with an intensity of 4–5 mW/cm^2 .

TOF and charge extraction via linearly increasing voltage (CELIV) measurements were carried out using a frequency-tripled Nd:YAG (yttrium aluminum garnet) laser (Solar System LQ129) at a wavelength of 532 nm and a pulse length of 10 ns. As the selected wavelength is located

near the fundamental absorption of the used PPV derivatives, electrode-near regimes of the thick organic layers were excited through the semitransparent cathode stack during TOF measurements. During CELIV measurements, however, the entire thin organic layer was excited. The transient current signals result from the motion of generated charge carriers under an applied voltage and were measured (in TOF and CELIV) by means of a current-voltage amplifier (Femto DHPA-100) and a digital oscilloscope (Tektronix TDS 5052). A few hundred consecutive current transients were averaged in order to decrease the noise level.

Charge carrier injection during TOF measurements was prevented by biasing the devices reversely. This is of importance, since most of the employed contacts provide efficient electron and hole injection from the cathode and the anode in forward bias, respectively. Hole currents were measured by irradiating through the positively biased, semitransparent cathode stack. For hole-only samples comprising PEDOT:PSS as anode and gold as cathode, charge carrier injection could not be prevented during TOF measurements. In general, the laser light intensity was adapted to ensure the small signal case where the optically generated charge is much smaller than CV of the sample, where C is the sample capacitance and V the voltage applied to the device.

For CELIV measurements a linearly increasing voltage was generated by means of a function generator (HP33120A). The voltage ramp started at an offset bias compensating for the built-in potential to maintain flatband conditions at the moment of photoexcitation. Then the voltage was decreased linearly (reversely biased) to drive the photo-generated carriers out of the organic layer. The magnitude of the voltage ramp changed from measurement to measurement by changing the frequency of the signal while maintaining the amplitude of the voltage constant. A delay timer controlled the time interval between the laser pulse arrival and the start of the voltage rise. The laser light penetrates the transparent anode and excites the whole PPV-layer of the thin-film OLEDs uniformly.

A previously developed one-dimensional drift-diffusion model of charge transport and injection in OLEDs is used to simulate the dc electrical response of the diodes used here.^{14,15,36}

III. RESULTS

Hole current transients for the three different PPV derivatives are depicted in Fig. 1 exemplarily. The thick (up to 2000 nm) OLED-like devices with the sandwich structure ITO/PEDOT:PSS/PPV/Ca/Al (for energetic scheme, see the inset of Fig. 4) were biased reversely with a voltage of 40 V during TOF measurements to prevent charge carrier injection. Such a bias results in similar internal electric fields of 212 kV/cm for OC₃C₈-PPV and OC₁C₁₀-PPV-based devices and 248 kV/cm for devices out of OC₈C₈-PPV. For the symmetric PPV, the current traces show an incompletely developed plateau. This plateau becomes less pronounced for OC₃C₈-PPV and for the most unsymmetrical representative of PPV, OC₁C₁₀-PPV, the plateau vanishes almost completely resulting in a featureless current decay. For devices

containing OC₁C₁₀-PPV, a characteristic decay time can only be identified in a double logarithmic representation, which is shown in the inset of Fig. 1. Such a featureless decay is characteristic for dispersive transport,¹⁶ where carrier relaxation in the broad density of states distribution of the polymer leads to a decay of the carrier speed during the transit.¹⁷ The transit time of the fastest charge carriers is marked by a characteristic current break-in where the incipient carrier loss by ejection at the counter electrode sets in. Linear fits were applied to the current transients before and after this characteristic time in the double logarithmic plot, and from the intersection of the fits the transit time τ of the fastest holes was extracted.¹⁶ From the data shown in Fig. 1 transit times of $\tau(\text{OC}_8\text{C}_8\text{-PPV}) = 8.4 \mu\text{s}$, $\tau(\text{OC}_3\text{C}_8\text{-PPV}) = 75 \mu\text{s}$, and $\tau(\text{OC}_1\text{C}_{10}\text{-PPV}) = 223 \mu\text{s}$ could be extracted. In the small signal case, the associated charge carrier mobility μ is given by

$$\mu = \frac{d^2}{(V - V_{bi})\tau} \quad (1)$$

with the thickness d of the organic layer, V the applied voltage and V_{bi} the built-in voltage, which can be estimated from the difference in the work functions of the electrode materials PEDOT:PSS and calcium to $V_{bi} = 2.3 \text{ V}$. For the data depicted in Fig. 1 and an extraction bias of $V = -40 \text{ V}$ mobilities of $\mu(\text{OC}_8\text{C}_8\text{-PPV}) = 8.1 \cdot 10^{-5} \text{ cm}^2/\text{Vs}$, $\mu(\text{OC}_3\text{C}_8\text{-PPV}) = 1.26 \cdot 10^{-5} \text{ cm}^2/\text{Vs}$, and $\mu(\text{OC}_1\text{C}_{10}\text{-PPV}) = 4.24 \cdot 10^{-6} \text{ cm}^2/\text{Vs}$ were found. It is apparent that fastest hole transport takes place in the material with the most symmetric side chains in agreement with the finding of others.¹⁸ A high degree of regularity can significantly increase the mobility due to the decrease of energetic disorder. The field dependence of the hole mobility of all three PPV derivatives measured with TOF using the unfatigued OLED-like structures is shown with filled symbols in the left plot of Fig. 3. For a hopping transport through amorphous organic semiconductors with a Gaussian density of states (DOS),¹⁹ the field de-

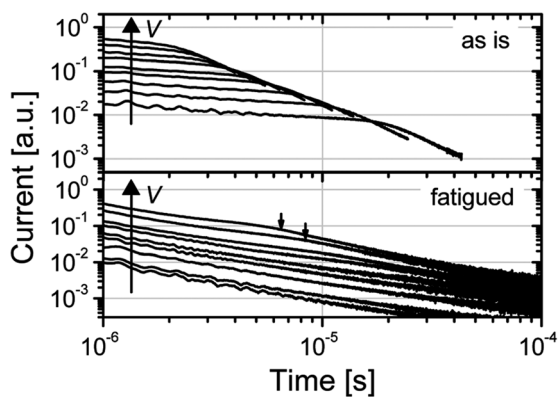


FIG. 2. Hole current transients for OC₈C₈-PPV before (upper plot) and after (lower plot) electrical fatigue in double logarithmic scale. The device structure was ITO/PEDOT:PSS/OC₈C₈-PPV(1.7 μm)/Ca. The measurements were carried out at voltages from 20 V to 100 V in reverse bias, the big arrows indicate the direction of increasing the absolute voltage. The transit times after three hours of electrical stress at a constant current density of $j = 10 \text{ mA}/\text{cm}^2$ are marked with small arrows.

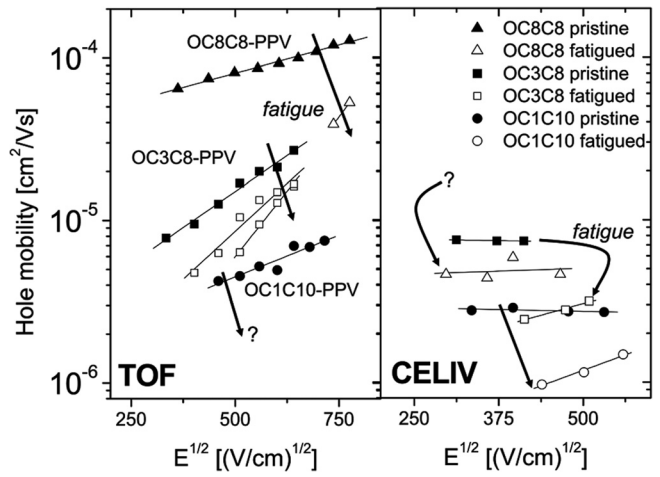


FIG. 3. Hole mobility of the three different PPV derivatives OC₈C₈ (triangles), OC₃C₈ (squares), and OC₁C₁₀-PPV (dots) before fatigue (filled symbols) and after electrical fatigue (open symbols) plotted over the square root of the internal electric field. Left plot: Hole mobilities before and after fatigue extracted from TOF measurements. Mobilities after fatigue can only be understood as upper limits as the transport became dispersive. Due to the strong dispersion of transport in OC₁C₁₀-PPV, transit times could not be detected after fatigue. For OC₃C₈-PPV, an additional fatigue step was executed, resulting in further reduced mobility values. Right plot: Mobilities extracted from photo-CELIV measurements. The hole mobility of OC₈C₈-PPV could not be detected with the CELIV method in the unfatigued sample. The arrows mark the evolution of the hole mobility during electrical fatigue. All device structures were ITO/PEDOT:PSS/PPV/Ca. Details regarding all the different PPV layer thicknesses and fatiguing conditions can be taken out of the text.

pendence of the charge carrier mobility at constant temperature can be given as

$$\mu = \mu^* \exp(\gamma\sqrt{E}) \quad (2)$$

with a zero field mobility μ^* and a field-factor γ . Both quantities depend on the energy disorder parameter characterizing the width of the density of states distribution. From Fig. 3 the zero field mobilities of $\mu^*(\text{OC}_8\text{C}_8\text{-PPV}) = 3.63 \cdot 10^{-5} \text{ cm}^2/\text{Vs}$, $\mu^*(\text{OC}_3\text{C}_8\text{-PPV}) = 2 \cdot 10^{-6} \text{ cm}^2/\text{Vs}$, and $\mu^*(\text{OC}_1\text{C}_{10}\text{-PPV}) = 1.38 \cdot 10^{-6} \text{ cm}^2/\text{Vs}$ were found while the coefficients were determined to be $\gamma(\text{OC}_8\text{C}_8\text{-PPV}) = 6.9 \cdot 10^{-4} (\text{cm}/\text{V})^{1/2}$; $\gamma(\text{OC}_3\text{C}_8\text{-PPV}) = 1.73 \cdot 10^{-3} (\text{cm}/\text{V})^{1/2}$; $\gamma(\text{OC}_1\text{C}_{10}\text{-PPV}) = 1.03 \cdot 10^{-3} (\text{cm}/\text{V})^{1/2}$. Referring to the results obtained for OC₁C₁₀-PPV, comparable values have been published by others.²⁰

In principle, the time-of-flight technique allows for the determination of both the hole and electron mobility.²¹ However, electron transport in PPVs is governed by the capture of electrons in deep traps, impeding the determination of the effective charge carrier mobility for electrons by time-of-flight measurements.^{22–24}

After the initial characterization of the unfatigued thick OLED-like structures, the devices were electrically stressed. Samples comprising OC₈C₈-PPV and OC₁C₁₀-PPV were operated with a constant current density of $j = 10 \text{ mA}/\text{cm}^2$ in forward bias resulting in an increase of the driving voltage from 150 V to 270 V in three hours and to 230 V in 30 minutes for OC₈C₈-PPV and OC₁C₁₀-PPV, respectively. Concomitantly, the luminescence decreased to 10% (or less

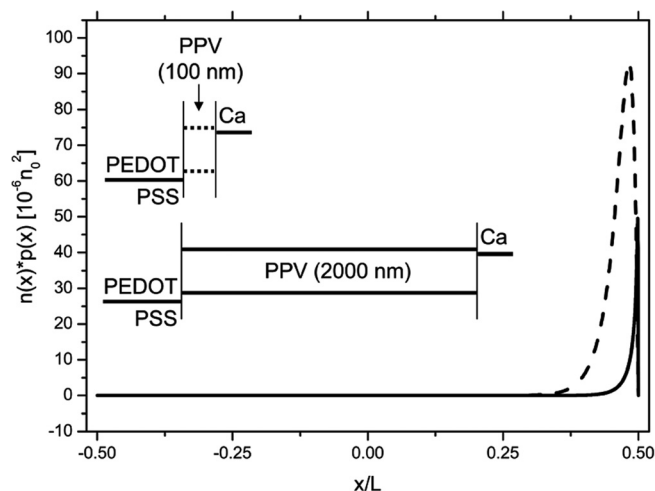


FIG. 4. Spatial distribution of the recombination zone determined by $n \cdot p$ for two different layer thicknesses $L = 100$ nm (dashed line) and $L = 2$ μm (solid line), calculated for a current density of $j = 50$ mA/cm^2 , barrier heights of $\Delta_p^- = \Delta_n^+ = 0.2$ eV and mobilities of $\mu_p = 100 \cdot \mu_n = 10^{-4}$ cm^2/Vs (Refs. 25 and 26). The anode is located at the left side starting at $x/L = -0.5$, the cathode on the right side starting at $x/L = 0.5$. The inset depicts the energetic schemes of the two different types of devices.

for OC_1C_{10} -PPV) of its initial value. A possible reason for this extraordinary fast decay is the high power influx during the operation of the thick devices. At the beginning of the stressing steps, the power reached 150 mW, which is five times higher than the power released in thin-film OLEDs. The thick OLED-like structures out of OC_3C_8 -PPV were therefore stressed more gently applying a constant voltage of 100 V, resulting in very small driving currents below 180 nA/cm^2 . During fatigue, the current densities decreased to 50 nA/cm^2 after 18 hours of operation and to 20 nA/cm^2 after 100 hours stressing. In these time ranges, the luminescence was reduced to 35% and 15% of its initial value, respectively. The power released was thus below 1.8 μW .

After each fatiguing step TOF measurements were repeated. In Fig. 2 the resulting hole current transients for an OLED-like sample out of OC_8C_8 -PPV are depicted for different electric fields in a double logarithmic plot. The transients can be compared with the respective transients of the unfatigued sample also depicted in Fig. 2. Distinct sudden decays of the displacement currents are visible for each electric field applied to the pristine device. Yet, the hole current transients look completely different after stressing the OLED (lower plot), characteristic times could only be identified for high electric fields, as marked with two small arrows. All other transients that were detected at lower electric fields showed a completely featureless decay even in the double logarithmic plot. The fact that the hole transients strongly decay with time indicates a relaxation of the carrier mobility that is not completed after the carrier transit. Consequently, the extracted hole mobilities are highly biased by the relaxation process and do not reflect the hole mobilities obtained from local equilibrium conditions. Transit times like for OC_8C_8 -PPV could be identified for OC_3C_8 -PPV even after a second fatiguing step. All transients of OC_1C_{10} -PPV samples, however, showed a completely featureless decay after stressing even in the double logarithmic plot.

The related hole mobility values were calculated out of the obtained transit times and are presented in the left part of Fig. 3. After fatigue (open symbols), the field dependence of the hole mobility was more pronounced and the hole mobility was reduced. The hole mobilities are characterized by $\mu^*(\text{OC}_8\text{C}_8\text{-PPV stressed}) = 1.26 \cdot 10^{-7}$ cm^2/Vs and $\gamma(\text{OC}_8\text{C}_8\text{-PPV stressed}) = 3.45 \cdot 10^{-3}$ $(\text{cm}/\text{V})^{1/2}$ for OC_8C_8 -PPV and $\mu^*(\text{OC}_3\text{C}_8\text{-PPV stressed1}) = 6.31 \cdot 10^{-7}$ cm^2/Vs ; $\mu^*(\text{OC}_3\text{C}_8\text{-PPV stressed2}) = 1.58 \cdot 10^{-7}$ cm^2/Vs ; $\gamma(\text{OC}_3\text{C}_8\text{-PPV stressed1}) = 2.36 \cdot 10^{-3}$ $(\text{cm}/\text{V})^{1/2}$ and $\gamma(\text{OC}_3\text{C}_8\text{-PPV stressed2}) = 3.22 \cdot 10^{-3}$ $(\text{cm}/\text{V})^{1/2}$ for OC_3C_8 -PPV after electrical stressing. This clearly shows that the hole mobility is reduced, the field dependence of the mobility becomes more pronounced, and the hole transport becomes more dispersive due to the electrical operation.

IV. DISCUSSION

Hole transport of thick OLED-like devices is fading during fatigue. This raises the question whether the obtained results can be transferred to the usual thin-film organic light-emitting diodes. Such a comparison is only meaningful as long as the device state under electrical stress is identical for both devices since then the electrical stress will be distributed comparably. In Fig. 4 the spatial distribution of the recombination zone can be seen for a current density of $j = 50$ mA/cm^2 as calculated from a drift/diffusion model described elsewhere.^{14,15,36} Normalized to its thickness, the dotted curve represents the recombination zone within a PPV layer of 100 nm thickness, sandwiched between PEDOT:PSS on the left and calcium on the right side. The continuous line illustrates the same for a 20 times thicker PPV layer with $L = 2000$ nm. In both cases, the recombination zone is located near the cathode. Substantial recombination and therefore generation of excitons take place in only less than 5% of the PPV thickness for the thin-film OLED. On the one hand, this means that excitations exist in a rather narrow region close to the cathode that is merely broadened by exciton diffusion.²⁷ On the other hand, it means that more than 95% of the entire PPV thickness is free of electrons and dominated by holes.¹⁵ Qualitatively this is similar for the 2000 nm thick device, where recombination takes place only in one percent of the layer thickness while 99% is free of electrons. Be aware that once the current density is reduced (not shown) the recombination region leaks deeper into the organic film. This change, however, occurs likewise for the thin-film devices and the TOF samples and does not exceed 10% of the entire layer thickness for the conditions investigated here. Since, for all examined operation conditions and device thicknesses, the bipolar, hole, and electron dominated regions are prorated, we conclude that a comparison between both devices is reasonable.

The transferability of the TOF results to thin-film OLEDs is experimentally investigated by comparing time-of-flight and photo-CELIV (photogenerated charge carrier extraction by linearly increasing voltage) measurements. CELIV is appropriate for obtaining information about the mobility of the fastest charge carrier species from thin-film diodes, although the method is relatively new and not studied

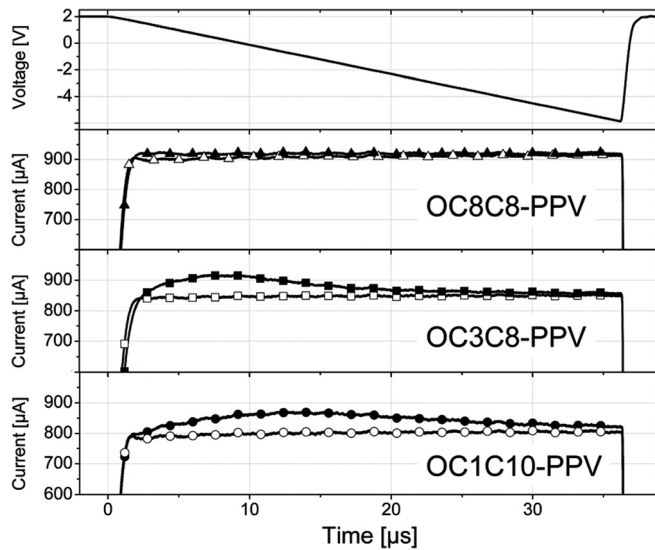


FIG. 5. Voltage ramp applied during a photo-CELIV measurement (uppermost graph) and resulting extraction currents (three lower graphs) without illumination (open symbols) and with previous (5 μs before start of voltage ramp) laser illumination (filled symbols). The extraction currents are shown for all three different PPV derivatives in the OLED configuration with calcium and ITO/PEDOT:PSS as electrodes and a layer thickness of 130 nm.

in every detail.²⁸ Exemplary current transients are depicted in Fig. 5 for pristine diodes based on all three PPV derivatives. The applied voltage ramp is shown in the uppermost plot. The diodes were initially biased in forward direction to compensate for the built-in voltage. After a time delay, the voltage decreased with a voltage decrease rate of $U' = -0.22 \text{ V}/\mu\text{s}$ and was finally reversely biased. Increasing the voltage linearly without previous laser illumination, plain horizontal currents (open symbols) are obtained. The independence of the dark current during the linear voltage increase indicates a weak injection current compared to the charging current of the diode plate capacitance. In comparison to these dark currents, the current transients for illuminated samples are depicted (filled symbols). The samples are illuminated by a short laser pulse with a wavelength within the fundamental absorption of the PPVs 5 μs before the voltage is increased. This excitation generates carriers in the entire PPV layer that are extracted thereupon by the increasing extraction bias. Thus, the extraction current due to photo-generated charge carriers in the organic layer is given by the difference of the current under illumination to the dark current. For unfatigued OC₈C₈-PPV based diodes, no apparent difference between both currents is observed. A possible reason for this missing extraction current could be a very fast extraction due to the large hole mobility (from TOF one obtains $10^{-4} \text{ cm}^2/\text{Vs}$), too fast to be detected. In the cases of OC₃C₈-PPV and OC₁C₁₀-PPV, the difference is more pronounced and maxima in the extraction currents can be identified at characteristic times of $t_{\text{max}}(\text{OC}_3\text{C}_8\text{-PPV}) = 8.2 \mu\text{s}$ and $t_{\text{max}}(\text{OC}_1\text{C}_{10}\text{-PPV}) = 13.5 \mu\text{s}$. From these characteristic times, the drift mobility of the extracted charge carriers in a photo-CELIV measurement can be determined by²⁹

$$\mu = \frac{2d^2}{3U't_{\text{max}}^2(1 + 0.36\Delta j/j_0)} \quad (3)$$

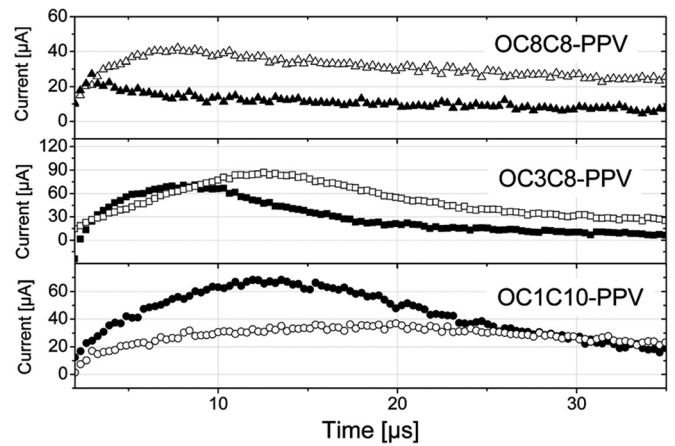


FIG. 6. Extraction currents obtained from photo-CELIV measurements, calculated as difference between currents after pulsed illumination and dark currents. For all three different PPV derivatives, the extraction currents are shown for pristine (filled symbols) and electrically fatigued (open symbols) devices. The devices were fatigued at constant current density of $j = 50 \text{ mA}/\text{cm}^2$ for 24 hours (OC₁C₁₀ and OC₃C₈-PPV) and 40 hours (OC₈C₈-PPV), respectively. The device structures were ITO/PEDOT:PSS/PPV(130 nm)/Ca. Laser illumination started 5 μs before the start of the applied voltage ramp, which was the same as shown in Fig. 5.

with the dark current j_0 and Δj the difference between dark and light current at t_{max} . For the examples depicted in Figs. 5 and 6, $\mu(\text{OC}_3\text{C}_8\text{-PPV}) = 7.4 \cdot 10^{-6} \text{ cm}^2/\text{Vs}$ and $\mu(\text{OC}_1\text{C}_{10}\text{-PPV}) = 2.73 \cdot 10^{-6} \text{ cm}^2/\text{Vs}$ were obtained. These values have the same order of magnitude as the mobilities extracted from the TOF experiments.

CELIV provides also information about the dispersive nature of transport.³⁰ The ratio of the characteristic time $t_{1/2}$ where the extraction current is decayed to half of its maximum and the time of the extraction current maximum t_{max} , has been provided as figure of merit characterizing the dispersive nature of the carrier transport. Thus, the broader an extraction current peak is, the more dispersive the transport should be. The broadest peak in the extraction currents for pristine devices is detected for the OC₁C₁₀-PPV-based device, which is in line with the highly dispersive transients observed in TOF experiments.

Subsequently to CELIV measurements on pristine OLEDs, the devices were operated at a constant current density of $50 \text{ mA}/\text{cm}^2$. Due to the device stress, the luminescence from OC₈C₈-PPV based thin-film diodes decreased in 40 hours to 70% of its initial value. For OC₃C₈-PPV and OC₁C₁₀-PPV-based diodes, 64% and 63% of the EL intensities were retained after 24 hours of operation. From the CELIV currents depicted in Fig. 6, one recognizes that the extraction current transients changed for all three PPV derivatives due to the electrical stress. While it was impossible to identify a clear extraction current maximum for the pristine OC₈C₈-PPV, a clear maximum at $t_{\text{max}}(\text{OC}_8\text{C}_8\text{-PPV stressed}) = 9.3 \mu\text{s}$ could be identified after fatigue. For the other two materials, the maxima shifted to larger times of $t_{\text{max}}(\text{OC}_3\text{C}_8\text{-PPV stressed}) = 13.3 \mu\text{s}$ and $t_{\text{max}}(\text{OC}_1\text{C}_{10}\text{-PPV stressed}) = 18.5 \mu\text{s}$. Accordingly, the associated mobilities are reduced to $\mu(\text{OC}_8\text{C}_8\text{-PPV stressed}) = 5.84 \cdot 10^{-6} \text{ cm}^2/\text{Vs}$, $\mu(\text{OC}_3\text{C}_8\text{-PPV stressed}) = 2.79 \cdot 10^{-6}$

cm^2/Vs , and $\mu(\text{OC}_1\text{C}_{10}\text{-PPV stressed}) = 1.48 \cdot 10^{-6} \text{ cm}^2/\text{Vs}$. Moreover, all extraction current peaks were broadened due to fatigue, which is a hint for a more dispersive transport.³⁰

The hole mobilities extracted out of CELIV measurements are depicted in the right graph of Fig. 3 in dependence of the square root of the internal electric field. Since the electric field in CELIV measurements changes in the progression of the carrier extraction, the time averaged electric fields were determined. These can be taken at $t \approx t_{\text{max}}$.²⁹ Even though absolute values differ, all tendencies of the evolution of the hole mobilities found by TOF measurements are reflected in the results obtained by CELIV. The hole mobility of the symmetric $\text{OC}_8\text{C}_8\text{-PPV}$ is the highest while it is the lowest in $\text{OC}_1\text{C}_{10}\text{-PPV}$. The transport in pristine $\text{OC}_1\text{C}_{10}\text{-PPV}$ is moreover the most dispersive of all pristine samples. After fatigue, the hole mobilities are reduced, the transport seems more dispersive and the field dependency is more pronounced.

In bipolar PPV-based OLEDs, the recombination region is close to the cathode (see Fig. 4). Hence, one could come to the conclusion that the fatigue occurs primarily within the large hole dominated volume fraction of the organic layer, through which the holes have to transit in order to reach the recombination zone. Thus, a comparable fatiguing would be expected for a hole only device where the electron injection is suppressed by exchanging the low work function cathode calcium for the high work function metal gold. On such ITO/PEDOT:PSS/ $\text{OC}_8\text{C}_8\text{-PPV}$ (2900 nm)/Au samples TOF measurements in the pristine and fatigued state were performed. These unipolar hole-only devices were fatigued by applying 300 V, resulting in hole current densities of around $50 \mu\text{A}/\text{cm}^2$. No change in the hole transients before and after fatigue for several days was found, indicating that hole current alone does not fatigue the hole transport. Hence, hole transport itself also cannot be responsible for the change in hole transport properties during bipolar electric fatigue. This is in accordance to previously mentioned results by Parker *et al.*⁵ Yet, from the energetic scheme depicted in the upper inset of Fig. 7, one recognizes that in such hole-only devices hole injection cannot be prevented, which complicates the TOF measurements due to injected carriers persisting in the organic layer. During the here performed TOF measurements a dc injection current in the range of $j = 10\text{--}100 \mu\text{A}/\text{cm}^2$ was flowing, 10 to 100 times higher than in usual TOF signals. Thus, the electric field and charge carrier distribution within the organic layer is unknown, and we refrained to extract transit times and mobility for this type of device. More severely, a dc charge carrier distribution within the organic layer will partially fill the available states thus deactivating crucial deep traps. A fatigue induced appearance of deep traps would thus be camouflaged and might be invisible for TOF. Yet, due to the fact that the dc hole injection current did not substantially change due to electrical stress the invariance of the TOF signal to fatigue in hole-only devices seems conclusive.

Beside a hole-related fatigue mechanism, a mechanism related to the internal electric field that is present between the electrodes during device operation might prevail. To investigate whether this holds true for the here investigated

PPV-based diodes, electron and hole blocking contacts out of Al were employed. They prevent injection of carriers in the typical TOF device structure during electrical stress, so that the influence of the electrical field can be studied separately. Due to the blocking nature of the contacts, the current densities were reduced to below $j = 80 \text{ nA}/\text{cm}^2$, while the samples were stressed by applying a voltage of 150 V resulting in electric fields of around $750 \text{ kV}/\text{cm}$. No change in the hole transients (not shown) could be observed once such an electric field has been applied for 43 hours. Thus, an electric field alone does not relate to the observed degradation of the hole transport during operation of OLEDs.

Since in any bipolar device recombination leads to the creation of excited molecules, the extended period of excitation during the device operation might harm the organic semiconductor and thus alter the device performance. To investigate whether excitonic states are responsible for the impeded hole transport properties, the TOF test structures Al/ $\text{OC}_8\text{C}_8\text{-PPV}$ /Al and ITO/PEDOT:PSS/ $\text{OC}_8\text{C}_8\text{-PPV}$ /Al were stressed optically by irradiating through the semitransparent aluminum while keeping the devices in an open-circuit condition. The latter condition ensures a negligible light-induced charge carrier generation because the device is held close to the flatband condition preventing field assisted exciton dissociation. Hence, little photo current and little photo carriers, but a substantial density of excitons was induced. LEDs with peak emission wavelengths of $\lambda = 516 \text{ nm}$ and $\lambda = 572 \text{ nm}$ and intensities of $4.1 \text{ mW}/\text{cm}^2$ and $4.7 \text{ mW}/\text{cm}^2$ were chosen for irradiation. The former wavelength lies in the fundamental absorption of the employed PPVs while the latter matches the overlap region of the photoluminescence and the absorption spectra of $\text{OC}_8\text{C}_8\text{-PPV}$. Considering that 60–80% of the irradiated light was reflected by the semitransparent cathode, the injected intensities seem to be in a similar range as the light intensity generated by an OLED. The absorption and emission spectra of $\text{OC}_8\text{C}_8\text{-PPV}$ are shown in the lower inset in Fig. 7, where the two different wavelengths used for optical fatigue are marked with vertical lines. Due to the strong absorbance at wavelengths of fundamental absorption, 90% of the light with $\lambda = 516 \text{ nm}$ is absorbed after 80 nm of PPV and 99% is absorbed after 160 nm. Light with $\lambda = 572 \text{ nm}$ penetrates deeper into the organic layer. 90% is absorbed after 270 nm while 1% reaches even 550 nm deep into the device. After irradiating the devices for several weeks with each of the LEDs, no change in hole current transients could be detected, compared to the hole currents of pristine samples (not shown). The sole existence of excitons does not cause a degradation of the hole transport properties of PPV-based OLEDs.

Finally, the origin of the fatigue of the hole transport could be related to the presence of electrons in the PPV layer. Apart from the investigated OLED-like samples, electrons were absent during the fatiguing steps applied to all other investigated TOF structures and none of these fatiguing steps led to a degradation of the hole transport properties as observed in the bipolar device. To generate electrons independently, the already investigated unipolar hole-only devices (ITO/PEDOT:PSS/ $\text{OC}_8\text{C}_8\text{-PPV}$ /Au) were irradiated through the semitransparent gold contact with the same

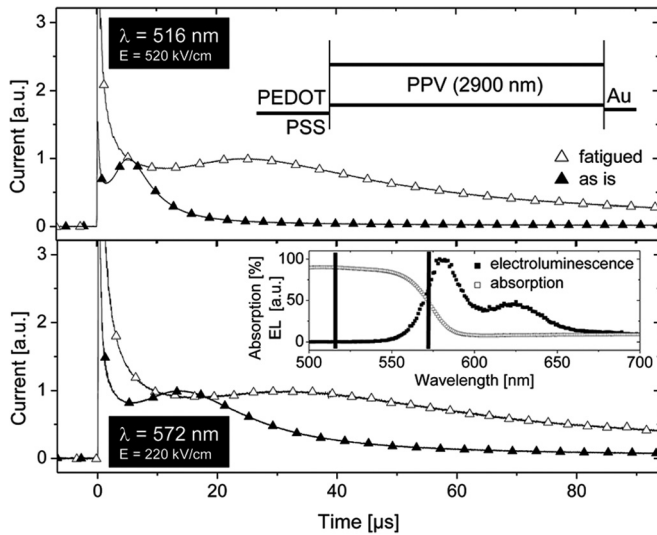


FIG. 7. TOF hole current transients of $\text{OC}_8\text{C}_8\text{-PPV}$ measured in two different devices with the sandwich structure ITO/PEDOT:PSS/ $\text{OC}_8\text{C}_8\text{-PPV}$ (2900 nm)/Au (energetic scheme shown in the upper inset) before (filled symbols) and after (open symbols) fatigue. Upper plot: TOF measurements at an electric field of 520 kV/cm. During fatigue for 22 hours a voltage of 300 V was applied while illuminating with a green LED ($\lambda = 516$ nm) through the semitransparent gold electrode. Lower plot: TOF measurements at an electric field of 220 kV/cm. During fatigue for 22 hours a voltage of 100 V was applied while irradiating with a yellow-green LED ($\lambda = 572$ nm) through the semitransparent gold electrode. All curves were normalized to their peak heights. The lower inset shows the absorption and emission spectra of $\text{OC}_8\text{C}_8\text{-PPV}$. The vertical lines mark the wavelengths of the LEDs used for optical fatigue.

LEDs as described above ($\lambda = 516$ nm and $\lambda = 572$ nm). This time, however, external biases of 300 V (for $\lambda = 516$ nm) or 100 V (for $\lambda = 572$ nm) were applied, leading to a photocarrier generation by electric field-induced exciton dissociation. Thus, the difference to a device stress by light at open circuit conditions or a device stress by applying a dc injection current lies in the additional presence of electrons. For both wavelengths, the devices were fatigued for 22 hours. Photo current densities of $50 \mu\text{A}/\text{cm}^2$ were reached during the fatiguing step independent of the wavelength. For a fatiguing wavelength of 516 nm, the hole transients before and after such a fatiguing variant can be seen in the upper plot of Fig. 7 for an electric field during TOF measurements of 520 kV/cm. For an irradiation with $\lambda = 572$ nm, the hole transients are depicted in the lower plot. Here carriers were extracted with an electric field of 220 kV/cm. Both devices exhibited a change in the hole transients after fatigue. In both cases the peaks, which are characteristic for the hole transients of hole-dominated devices without blocking contacts, became broader and shifted to longer times after fatigue (open symbols), indicating that the hole transport properties are affected by the employed fatiguing procedure. The fact that a change in hole transients can be induced by irradiating even with $\lambda = 572$ nm gives a hint that self-absorption could play a decisive role in the pure electrical device fatiguing since this wavelength is positioned directly in the overlap of emission and absorption spectra of the employed $\text{OC}_8\text{C}_8\text{-PPV}$ (see inset in Fig. 7). In thin film OLEDs, the light generated by carrier recombination and radiative decay of excitons will be subsequently reabsorbed when passing the

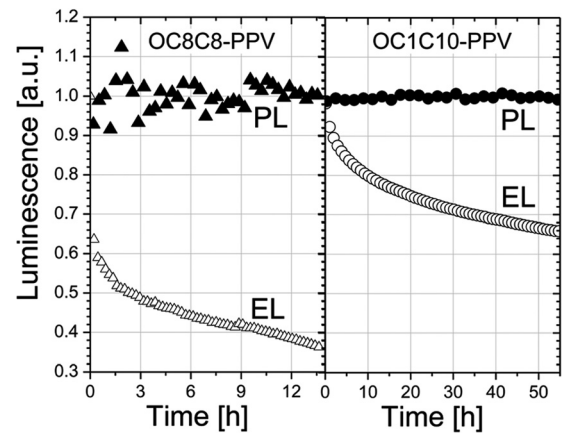


FIG. 8. Evolution of photoluminescence (filled symbols) and electroluminescence (open symbols) during electrical fatigue of OLEDs with $\text{OC}_8\text{C}_8\text{-PPV}$ (triangles) and $\text{OC}_1\text{C}_{10}\text{-PPV}$ (dots) as luminescent layers and layer thicknesses of $d = 130$ nm. PEDOT:PSS and calcium served as electrodes. The devices were stressed at a constant current density of $j = 100 \text{ mA}/\text{cm}^2$ for OC_8C_8 (left) and $j = 10 \text{ mA}/\text{cm}^2$ for OC_1C_{10} (right). The photo- and electroluminescence intensities were normalized to their initial values.

emissive layer. Because the penetration depth of light in PPVs is generally much larger than the width of the recombination zone, a material degradation over the entire PPV thin film is more likely than a localized degradation in the narrow electron dominated region of the OLED. Yet, this does not mean that most of the PPV molecules are degraded. This is demonstrated by the evolution of the photoluminescence intensity measured *in situ* during the operation of thin-film OLEDs with $\text{OC}_8\text{C}_8\text{-}$ and $\text{OC}_1\text{C}_{10}\text{-PPVs}$, shown in Fig. 8. The devices were stressed with a constant current density of $j = 100 \text{ mA}/\text{cm}^2$ and $j = 10 \text{ mA}/\text{cm}^2$, respectively. After 12 hours the electroluminescence intensity of the $\text{OC}_8\text{C}_8\text{-OLED}$ was decreased to less than 40% of the initial value while the more gently fatigued $\text{OC}_1\text{C}_{10}\text{-PPV}$ sample showed an electroluminescence intensity of more than 60% after 50 hours of operation. However, in both cases the photoluminescence remained unchanged. A degradation of a substantial amount of the PPV molecules during electrical operation seems therefore unlikely.

The transport and injection of charge carriers in PPV-based materials is well described by the correlated Gaussian disorder model as discussed by others.²⁵ For hopping transport along a Gaussian density of states distribution in an electric field, the temperature and field dependent mobility [see Eq. (2)] can be approximated as

$$\mu = \mu_{\infty} \exp \left[- \left(\frac{3\sigma}{5k_{\text{B}}T} \right)^2 + 0.78 \left(\left(\frac{\sigma}{k_{\text{B}}T} \right)^{\frac{3}{2}} - 2 \right) \sqrt{\frac{qaE}{\sigma}} \right] \quad (4)$$

with the Gaussian disorder parameter σ , the Boltzmann constant k_{B} , the infinite temperature zero field mobility μ_{∞} , the intersite spacing a , and the elemental charge q .^{19,31} According to the correlated Gaussian disorder model, a higher disorder results in a lower zero field mobility at constant temperature and in a stronger field dependence of the carrier mobility just as observed for all three PPVs during fatigue.

This indicates that a critical change in the density of states distribution might be initiated by electrical stress. The stress-induced evolution of the Gaussian disorder parameter can be obtained by assuming the intersite spacing for the pristine materials to be $a = 1.2 \text{ nm}$ ¹⁸ and fitting equation (4) to the experimental TOF data (Fig. 3, left). For OC₈C₈-PPV, the fatigue induces a change from 57 meV to 115 meV while the intersite spacing is increased to $a = 1.9 \text{ nm}$. The infinite zero field mobility is $\mu_\infty = 2.3 \cdot 10^{-4} \text{ cm}^2/\text{Vs}$. For the two different fatiguing steps carried out at the OC₃C₈-PPV based OLED-like TOF samples, σ changed from 86 meV in the pristine device to 94 meV and 108 meV after subsequent electrical stressing. At the same time, the intersite spacing a did not change during the first fatiguing step, but was found to be 1.9 nm after the second stressing step and μ_∞ was identified to be $1.4 \cdot 10^{-4} \text{ cm}^2/\text{Vs}$. Such a substantial change in the effective σ while still leaving the majority of the molecules untouched requires the creation of states deep in the bandgap. Indeed, in Ref. 32, it is demonstrated that intentionally introduced deep traps lead to an increased transit time and a higher dispersivity of current transients in TOF measurements. In particular, this holds true for trap densities as low as in the ppm region. Nonetheless, a broadening of the density of states distribution due to electrical stress has still to be proved, e.g., by means of temperature dependent TOF or thermally stimulated current (TSC) measurements.

In general, a broadening of the density of states distribution is also in line with an enhanced dispersiveness of transport.^{17,19,32,33} A broadening of the DOS leads to an increased relaxation time of photogenerated charge carriers towards the local equilibrium distribution.¹⁷ The carrier speed decreases during this relaxation process causing a fading current density in time. As long as the carrier distribution did not entirely relax after full transient, dispersive transport will be observed. As a consequence, a transition from nondispersive to dispersive transport can be initiated by an increase of the Gaussian disorder parameter σ , characterizing the DOS. Movaghar *et al.*^{34,35} determined a critical disorder parameter σ_c determining the transition between dispersive and nondispersive transport by comparing relaxation and transit times:

$$\frac{\sigma_c}{k_B T} = 1.22 \sqrt{\ln \left[\frac{6k_B T d}{q a^2 E} \right]}. \quad (5)$$

Here d is the total layer thickness of the PPV film. For the investigated device layouts and PPV derivatives, the critical width of the DOS at room temperature is in the range of 90 meV. Considering the evolution during the fatiguing process, it becomes apparent that a transition to dispersive transport occurs.

V. CONCLUSION

The hole transport properties in PPV-based OLED-like structures were investigated before and after electrical stress with the time-of-flight technique. A decrease in hole mobility, an increase in the field dependency of the hole mobility, and a transition to more dispersive transport were observed due to fatigue for all investigated PPV derivatives. In rela-

tion to the common correlated Gaussian disorder model applying to the transport in PPV-based materials, this evolution of the hole transport properties suggests an increase of the disorder parameter and thus a broadening of the density of states distribution. TOF measurements on various PPV-based derivatives in relation to different variants of electrical and optical fatiguing revealed that the presence of electrons is required to fatigue the hole transport. This is surprising since it is established that most of the PPV OLEDs are hole dominated and should thus be free of electrons at least in a substantial volume fraction. However, comparable optical fatiguing in hole dominated PPV devices was demonstrated by emulating a reabsorption process. This indicates that reabsorption of light generated in the recombination zone of an operating OLED might provide the electrons required for fatigue all over the PPV layer. Since it was demonstrated that our findings can be transferred to thin-film devices, the presented results are highly relevant for the fatigue behavior of PPV-based OLEDs.

ACKNOWLEDGMENTS

This work was supported by the Deutsche Forschungsgemeinschaft (DFG) through Sonderforschungsbereich 595. The polymers OC₈C₈-PPV and OC₃C₈-PPV were synthesized in the group of Professor Rehahn, Ernst-Berl-Institut für Technische und Makromolekulare Chemie, TU Darmstadt.

- ¹D. Hertel, C. D. Müller, and K. Meerholz, *Chem. Unserer Zeit* **39**, 336 (2005).
- ²D. Braun and A. J. Heeger, *Appl. Phys. Lett.* **58**, 1982 (1991).
- ³R. H. Friend, R. W. Gymer, A. B. Holmes, J. H. Burroughes, R. N. Marks, C. Taliani, D. D. C. Bradley, D. A. Dos Santos, J. L. Bredas, M. Logdlund, and W. R. Salaneck, *Nature* **397**, 121 (1999).
- ⁴A. Kraft, A. C. Grimsdale, A. B. Holmes, *Angew. Chem. Int. Ed.* **37**, 402 (1998).
- ⁵I. D. Parker, Y. Cao, and C. Y. Yang, *J. Appl. Phys.* **85**, 2441 (1999).
- ⁶H. Aziz and G. Xu, *J. Phys. Chem. B* **101**, 4009 (1997).
- ⁷K. K. Lin, S. J. Chua, and W. Wang, *Thin Solid Films* **417**, 36 (2002).
- ⁸M. Yan, L. J. Rothberg, F. Papadimitrakopoulos, M. E. Galvin, and T. M. Miller, *Phys. Rev. Lett.* **73**, 744 (1994).
- ⁹S. Karg, J. C. Scott, J. R. Salem, and M. Angelopoulos, *Synth. Met.* **80**, 111 (1996).
- ¹⁰B. H. Cumpston, I. D. Parker, and K. F. Jensen, *J. Appl. Phys.* **81**, 3716 (1997).
- ¹¹S. A. Carter, M. Angelopoulos, S. Karg, P. J. Brock, and J. C. Scott, *Appl. Phys. Lett.* **70**, 2067 (1997).
- ¹²J. C. Scott, J. H. Kaufman, P. J. Brock, R. DiPietro, J. Salem, and J. A. Goitia, *J. Appl. Phys.* **79**, 2745 (1996).
- ¹³J. Dane and J. Gao, *Appl. Phys. Lett.* **85**, 3905 (2004).
- ¹⁴F. Neumann, Y. A. Genenko, C. Melzer, and H. von Seggern, *J. Appl. Phys.* **100**, 084511 (2006).
- ¹⁵S. V. Yampolskii, Y. A. Genenko, C. Melzer, K. Stegmaier, and H. von Seggern, *J. Appl. Phys.* **104**, 073719 (2008).
- ¹⁶H. Scher and E. W. Montroll, *Phys. Rev. B* **12**, 2455 (1975).
- ¹⁷L. Pautmeier, R. Richert, and H. Bässler, *Philos. Mag. Lett.* **59**, 325 (1989).
- ¹⁸H. C. F. Martens, P. W. M. Blom, and H. F. M. Schoo, *Phys. Rev. B* **61**, 7489 (2000).
- ¹⁹H. Bässler, *Phys. Status Solidi B* **175**, 15 (1993).
- ²⁰P. W. M. Blom, M. J. M. de Jong, and M. G. van Munster, *Phys. Rev. B* **55**, 656 (1997).
- ²¹P. M. Borsenberger and D. Weiss, *Organic Photoreceptors for Xerography* (Marcel Dekker, New York, 1998).
- ²²H. Antoniadis, M. A. Abkowitz, and B. R. Hsieh, *Appl. Phys. Lett.* **65**, 2030 (1994).

- ²³P. W. M. Blom, M. J. M. de Jong, and J. J. M. Vleggaar, *Appl. Phys. Lett.* **68**, 3308 (1996).
- ²⁴M. M. Mandoc, B. de Boer, and P. W. M. Blom, *Phys. Rev. B* **73**, 155205 (2006).
- ²⁵P. W. M. Blom and M. C. J. M. Vissenberg, *Mater. Sci. Eng. R.* **27**, 53 (2000).
- ²⁶P. W. M. Blom and M. J. M. de Jong, *Philips J. Res.* **51**, 479 (1998).
- ²⁷D. E. Markov, E. Amsterdam, P. W. M. Blom, A. B. Sieval, and J. C. Hummelen, *J. Phys. Chem. A* **109**, 5266 (2005).
- ²⁸G. Juska, K. Arlauskas, M. Viliunas, and J. Kocka, *Phys. Rev. Lett.* **84**, 4946 (2000).
- ²⁹G. Juska, K. Arlauskas, M. Viliunas, K. Genevicius, R. Österbacka, and H. Stubb, *Phys. Rev. B* **62**, R16235 (2000).
- ³⁰G. Juska, N. Nekrasas, K. Genevicius, J. Stuchlik, and J. Kocka; *Thin Solid Films* **451**, 290 (2004).
- ³¹S. V. Novikov, D. H. Dunlap, V. M. Kenkre, P. E. Parris, and A. V. Vannikov, *Phys. Rev. Lett.* **81**, 4472 (1998).
- ³²A. Fleissner, H. Schmid, C. Melzer, and H. v. Seggern, *Appl. Phys. Lett.* **91**, 242103 (2007).
- ³³P. M. Borsenberger, L. T. Pautmeier, and H. Bässler, *Phys. Rev. B* **46**, 12145 (1992).
- ³⁴B. Movaghar, B. Pohlmann, and D. Würtz, *J. Phys. C* **14**, 5217 (1981).
- ³⁵B. Movaghar, M. Grünewald, M. Ries, H. Bässler, and D. Würtz, *Phys. Rev. B* **33**, 5545 (1986).
- ³⁶Yu. A. Genenko, S. V. Yampolskii, C. Melzer, K. Stegmaier, and H. von Seggern, *Phys. Rev. B* **81**, 125310 (2010).